

Reciprocal-space up-sampling from real-space oversampling in x-ray ptychographyD. J. Batey,^{1,*} T. B. Edo,¹ C. Rau,² U. Wagner,² Z. D. Pešić,² T. A. Waigh,³ and J. M. Rodenburg^{1,4}¹*Department of Electronic and Electrical Engineering, University of Sheffield, S1 3JD, United Kingdom*²*Diamond Light Source Ltd., Harwell Science and Innovation Campus, Didcot, Oxfordshire OX11 0DE, United Kingdom*³*Photon Science Institute, University of Manchester, Oxford Road, Manchester, M13 9PL, United Kingdom*⁴*Research Complex at Harwell, Harwell Oxford, Didcot, Oxfordshire, OX11 0DE, United Kingdom*

(Received 6 August 2013; published 9 April 2014)

We retrieve x-ray phase images from ptychographical data which, according to the conventional coherent diffractive imaging (CDI) criterion, have been grossly undersampled. Ptychographical data are intrinsically oversampled in real space, as the illumination function of subsequent exposures overlap. By exploiting the real-space redundancy in ptychography, we are able to recover the conventional CDI reciprocal sampling, despite an increase in the solid angle of the detector pixels. As a result the current experimental geometrical constraints placed upon probe size, object to detector distance, and pixel size are all relaxed.

DOI: [10.1103/PhysRevA.89.043812](https://doi.org/10.1103/PhysRevA.89.043812)

PACS number(s): 42.30.Kq, 42.30.Va, 42.30.Rx

I. INTRODUCTION

By liberating x-ray imaging from x-ray optics, ptychography has already shown itself to have unique capabilities in imaging biological and complex inorganic structures (see, for example, Refs. [1–3]). It promises unmatched resolution and high-contrast phase image sensitivity, as well as elemental mapping capabilities [4,5], all of which are crucial for improving structural discovery of all types of matter. Unlike conventional coherent diffractive imaging (CDI), which uses a single diffraction pattern and *a priori* knowledge that the object is finite, in ptychography we can arrange for each point in the object to fall within the illuminating beam (sometimes called the probe) several times for different positions of the object relative to the probe, so that each element of the object contributes to at least two (and often many) of the collected diffraction patterns. A synthetic lens is generated by solving for the phase of each of these diffraction patterns using one of several reconstruction algorithms [6–8].

Until recently it has been assumed that in all CDI methods, including ptychography, the sampling condition in the diffraction plane (i.e., the required minimum angular size of the detector pixel subtended at the object plane) is predicated by the object or probe size. Indeed, since its first demonstration in 1999 [9], the phase problem in CDI has been discussed in terms of oversampling with respect to the underlying Nyquist detector sampling (NDS) of the complex-valued wave. This means that the diffraction pattern has to be sampled at twice the periodicity of the wave amplitude incident upon the detector because twice as many intensity measurements (real numbers) are required to solve for the complex-valued wave function (real and imaginary numbers) arriving at the detector [10]. Let us call this the conventional detector sampling (CDS), given by

$$\Delta\theta \leq \frac{\lambda}{2D}, \quad (1)$$

where D is the maximum lateral dimension of the object, or the illumination upon it (whichever is smaller), λ is the wavelength, and $\Delta\theta$ is the angle subtended at the specimen

by a detector pixel. We have shown elsewhere that in fact the overall sampling in ptychography (as distinct from single-shot CDI) is independent of probe size (D) [11].

In our earlier work [11] we examined this issue with sparse sampling in the detector plane; the detector pixels employed were small relative to their separation distances, reflecting the equivalence of the discrete sampling of the probe positions in real space. Here we examine the case of recovering undersampled diffraction data collected using a real detector, wherein each pixel integrates a substantial area of the scattered intensity. If the characteristic size of the structure of the diffraction pattern is very small (the probe size is large), at first it may be thought that the integration process will obliterate any useful information. However, it must be remembered that the intensity at each (large) pixel is measured many more times as the distance between scan positions in real space is reduced: This implicit information can be used to fabricate a synthetic detector which at least meets the NDS criterion, inferring what would have been measured on such a detector had it physically existed. Our approach up-samples a coarse detector into one with notionally many more, much finer, pixels which can measure the complex-valued diffraction pattern. A finely sampled reciprocal-space diffraction pattern provides a much larger Fourier-repeat unit cell in real space, which can accommodate a much larger probe than can be handled, according to Eq. (1), by the pixel size of the physical detector. The effects of large detector pixels have been alleviated in conventional CDI with the addition of a subpixel scan of the detector during data acquisition [12]. Our method removes the need for any alterations to the physical setup and the sample's radiation dose and reduces the total amount of data required for the reconstruction.

Being able to use a much larger probe in a ptychographic experiment has important consequences. Although some workers use highly focused illumination in ptychography [13], even a perfectly focused probe (of the form of an Airy disk) has extensive side lobes which exacerbate the requisite sampling in the diffraction plane. There are also many good reasons to have a probe which is not focused but in fact has complicated, or almost random, structure. With count-rate limited detectors it is often not possible to use all the flux of the beamline if

*elp10db@shef.ac.uk

the central region of the diffraction pattern is bright. By using a probe that produces a well-developed speckle pattern in the far field [5,14], a much higher total flux can be employed. Having a wide range of incident plane waves composing the probe, which are randomly dephased with respect to one another, can also be used to extend the effective numerical aperture of the detector using super-resolution methods [15] or to obtain depth-specific information [16]. Such probes are relatively large in the object plane, so that it becomes difficult to satisfy the CDS. In contrast, our approach relieves all the geometrical constraints on probe size and detector pixel size, so that the detector can be positioned very much closer to the specimen. Currently, the specimen-detector distance can be a serious experimental limitation, even in the case of a long experimental hutch, especially in the case of Bragg ptychography [17], where the detector lies at twice the Bragg angle and is therefore also constrained by the hutch height. Moreover, being able to move the detector substantially closer to the specimen allows a detector with a given number of pixels to capture much higher angles of scatter, recording much higher-resolution information.

II. EXPERIMENTAL

To compare our up-sampling approach with the sparse data configuration, we use the same data as reported in Ref. [11], which were collected at the I13 beamline at the Diamond Light Source with the experimental setup shown in Fig. 1. This beamline has been built unusually long so as to produce a large area of spatial coherence in the hutch ($100 \times 800 \mu\text{m}$ in the horizontal and vertical directions respectively) at hard x-ray energies [18]. The undulator gap was set to maximize the photon flux at 8.7 KeV ($\lambda = 0.14 \text{ nm}$) selected by a pseudochannel cut Si(111) crystal monochromator, with a spectral spread, $\Delta\lambda/\lambda$, of 10^{-4} . The illumination incident upon the specimen was created by a pair of slits orientated in the horizontal and vertical planes with gaps of 17 and $19 \mu\text{m}$ at distances of 45 and 24 mm upstream of the specimen respectively. The specimen was constructed from a 3-mm transmission electron microscope slot grid with a dispersion of 2.8- μm M-270 amine superparamagnetic

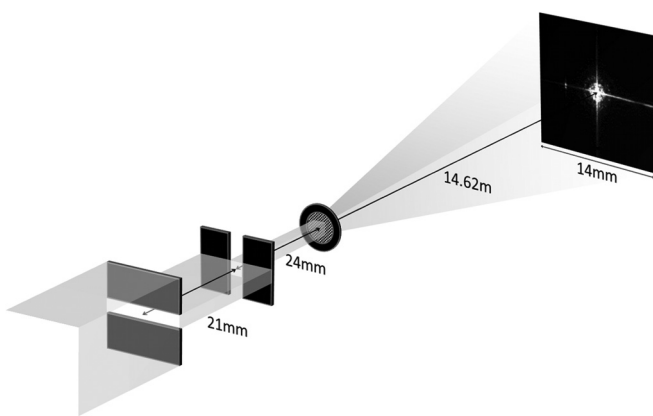


FIG. 1. Experimental setup: the beam propagates from the source (left) onto the two sets of slits, which forms a probe on the specimen forming an exit wave, which then further propagates onto the detector.

dynabeads on a carbon support film. The detector (a Maxipix TAA22PC composed of a 2×2 array of CCD chips each with 256×256 pixels of $55 \mu\text{m}^2$ [19]) was positioned 14.62 m downstream of the specimen. During the acquisition process, diffraction patterns were recorded (with 18 s of exposure each) as the specimen stage was scanned over a 32×32 grid with nominal probe-position separations of $6 \mu\text{m}$ and with random offsets of $0 \pm 0.3 \mu\text{m}$. To avoid the dead zones between chips, only a single quadrant of the detector (256×256 pixels) was used.

III. UP-SAMPLING METHOD

Using arguments relating to the number of measurements contributing to a dataset, we have defined a more general sampling framework that is better suited to ptychographic data [11]. The pertinent sampling condition is

$$\Delta\theta\Delta R \leq \frac{\lambda}{2}, \quad (2)$$

where ΔR is the approximate distance between probe positions in the object plane. It is useful to define

$$\hat{S}_{x,y} = \frac{\lambda}{2\Delta\theta\Delta R}, \quad (3)$$

which is a measure of how much the intensity of the ptychographical dataset has been oversampled above the requisite minimum, $\hat{S}_{x,y} = 1$, in each x - y direction. ($\hat{S}_{x,y}$ is twice the necessary sampling for the underlying complex-valued wave, $S_{x,y}$ [11].) As the sampling condition is of a reciprocal nature, we can compensate for undersampling in the detector plane by increasing the density of scan positions in real space. The information content of the experiment is conserved because reducing ΔR increases the number of diffraction patterns collected per object element. A surprising consequence of this analysis, exploited in this paper, is that Eq. (2) is independent of D : The illumination can be many times greater than that predicted by the conventional wisdom of CDI.

To investigate the effects of up-sampling, the actual dataset used here has been collected in a configuration that satisfies the conventional CDS, while the sampling in real space (ΔR , the illumination step size) is such that the ptychographic dataset is oversampled, giving $\hat{S}_{x,y} = 3.1$. We have then artificially binned the diffraction data by 2×2 and 3×3 pixels (in the horizontal and vertical directions), leading to gross CDS undersampling. However, we know that the underlying data is oversampled by a factor of 3.1×3.1 : just enough to recover the effects of the 3×3 binning.

We are now required to solve for 4 (2×2) or 9 (3×3) times more diffraction plane pixels than we have actually measured. Our reconstruction algorithm uses a more general reciprocal-space update step, similar in form to that described previously in the context of mixed states [20–22]. While the algorithm used here (which we call sPIE) is a generalization of the ePIE algorithm, the principle holds for any ptychographic reconstruction algorithm. The key step is to run the algorithm assuming a synthetic detector with the requisite number of pixels to satisfy the NDS criterion. As is usual in the ePIE algorithm, we start with a rough estimate of the (possibly very large) probe that exists within a Fourier-repeat unit cell

corresponding to the reciprocal of our synthetic detector pixel size. We form an estimate of the exit wave as usual (in this case assuming the multiplicative approximation, although the method would also apply to three dimensional [3-D] inversion methods [16]), and computationally propagate the resulting exit wave to the detector plane. In fact, we only have one experimental intensity measurement for the many synthetic detector pixels lying within it, but we nevertheless have forward calculation estimates of the complex-valued wave at all the synthetic pixels. The synthetic measurements are altered such that

$$\Psi'_{m,n} = \frac{\Psi_{m,n} \sqrt{I_m}}{\sqrt{\sum_{n=1}^N |\Psi_{m,n}|^2}}, \quad (4)$$

where Ψ and Ψ' represent the complex value at each synthetic pixel, before and after the update step respectively; I represents the intensity value of the recorded pixel; m addresses the recorded pixel coordinates; n addresses the synthetic subpixel coordinates; and N is the number of

synthetic subpixels per recorded pixel. In words, we have scaled the intensities of the synthetic pixels so that their sum matches the measured detector pixel intensity and then applied the modulus constraint to all the synthetic pixels as usual. For the case where N is 1, the sPIE update is identical to that in ePIE. Note that in Ref. [11], we investigated updating the modulus constraint from known (measured) data at widely spaced intervals in reciprocal space. Here we are solving for a multiplicity of virtual pixels within a single large detector pixel, none of which have been individually measured.

Each dataset is reconstructed with sPIE, alongside ePIE for comparison. All the initial illumination functions were modeled by propagating a plane wave through the two upstream slits according to their known distances from the object. All the initial object estimates were of free space. Figures 2, 3, and 4 show the diffraction pattern, phase image, and probe reconstructions respectively for various binning and up-sampling ratios. Table I lists, for each reconstruction, how much the original data was binned, its consequent underlying Ptychographical sampling (given ΔR , which is fixed for all the data used here), and how much the data have been up-sampled. The results show how sPIE is able to process the diffraction data

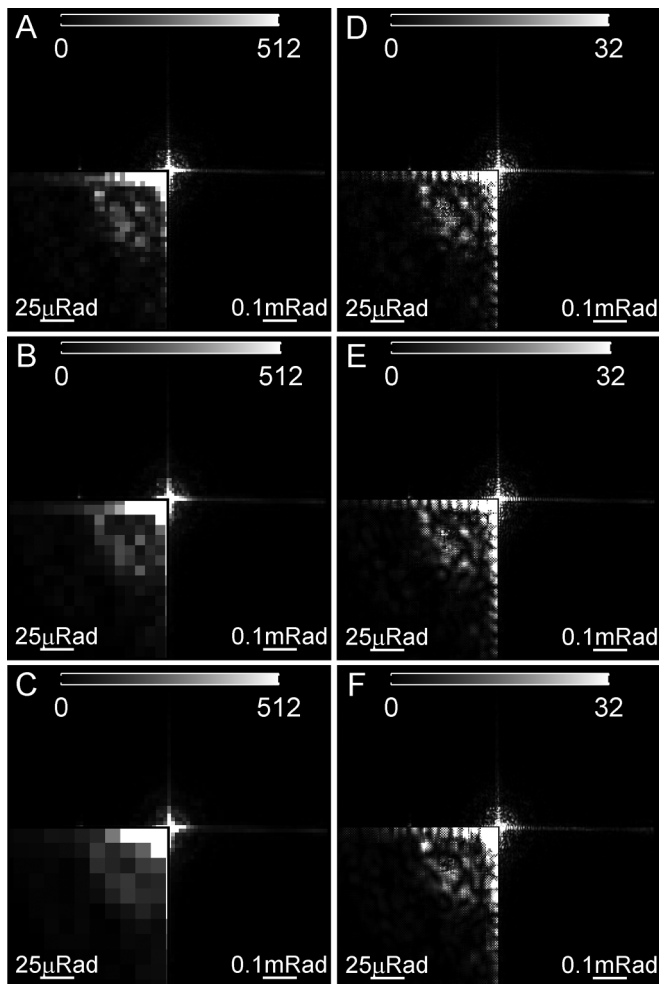


FIG. 2. Typical intensity patterns in the detector plane, with magnified inlays of the region beneath their top right corner. [Panels (a)–(c)] Recorded pattern binned by 1×1 , 2×2 , and 3×3 respectively; [panels (d)–(f)] recovered patterns after sPIE reconstructions with panels (a)–(c) as inputs up-sampled by 4×4 , 8×8 , and 12×12 respectively. The pixel range has been scaled here for display purposes.

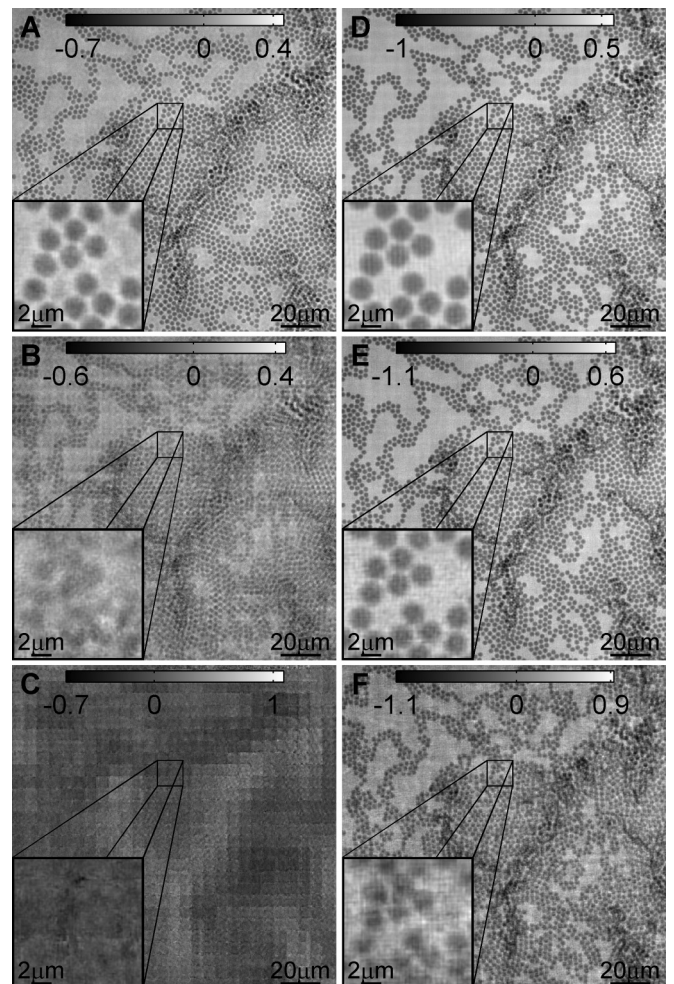


FIG. 3. Reconstructed phase images, with magnified inlays. [Panels (a)–(c)] ePIE reconstructions of data in Figs. 2(a)–2(c) respectively; [panels (d)–(f)] sPIE reconstructions of data in Figs. 2(a)–2(c) up-sampled by 4×4 , 8×8 , and 12×12 respectively.

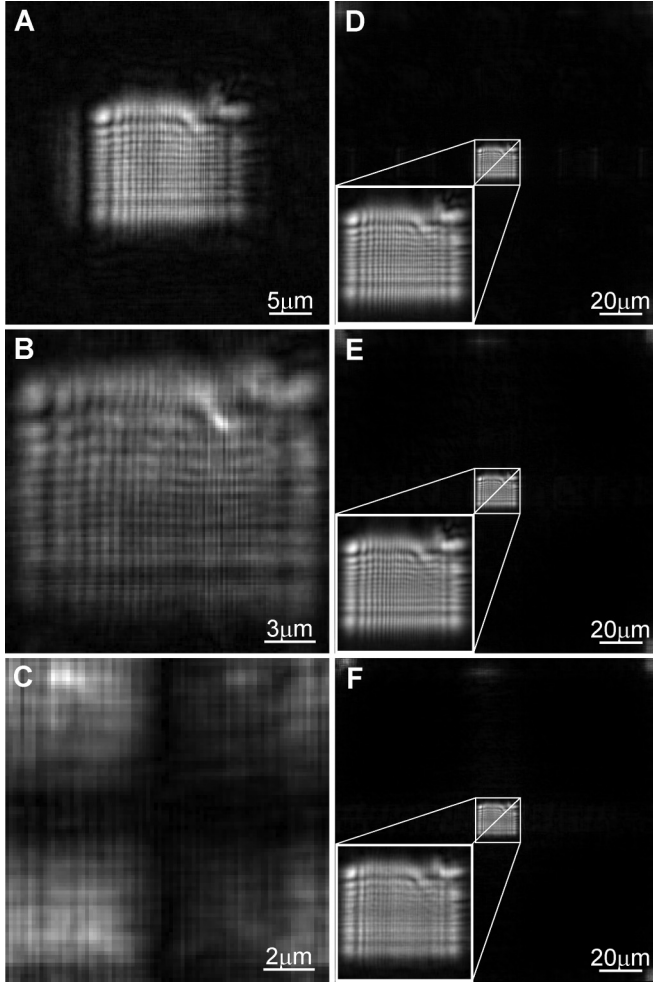


FIG. 4. Reconstructed illumination functions. [Panels (a)–(c)] ePIE reconstructions of data in Figs. 2(a)–2(c) respectively; [panels (d)–(f)] sPIE reconstructions of data in Figs. 2(a)–2(c) up-sampled by 4×4 , 8×8 , and 12×12 respectively.

down to a binning factor of 3×3 and up-sample that data by a factor of 12×12 , thus solving for 144 times as many synthetic pixels as measured pixels. ePIE clearly begins to break down when the CDS binning increases only to a factor of 2×2 . sPIE degrades significantly at a CDS binning of 4×4 (not shown),

TABLE I. A comparison of the various levels of conventional and ptychographic sampling ratios of each dataset along with the total up-sampling ratio achieved for each.

Figs. 2–4	$\sigma_{x,y}^a$	$\hat{S}_{x,y}^b$	$\eta_{x,y}^c$
a	1	3.1	1
b	$\frac{1}{2}$	1.6	1
c	$\frac{1}{3}$	1.0	1
d	1	3.1	4
e	$\frac{1}{2}$	1.6	8
f	$\frac{1}{3}$	1.0	12

^aCDI sampling ratio.

^bPtychographic sampling ratio.

^cUp-sampling ratio.

but this is expected because the underlying ptychographic sampling factor ($\hat{S}_{x,y}$) for the recorded dataset is just 3.1.

Interestingly, as long as the data satisfy Eq. (2), we can in principle up-sample by as many factors as we desire. This is demonstrated in Fig. 3(f), where data with $\hat{S}_{x,y}$ just over 1 is up-sampled by a factor of 12×12 . The illumination function is now embedded in a Fourier-repeat unit cell which has 64 times the area of the probe itself [Figs. 4(d)–4(f)]. We have so far found that the only practical upper limit of the probe size is governed by the area covered by the scan positions: These should cover at least twice the size of the probe in each direction in order for the dataset to have enough information to converge on both the object and probe function. This condition is independent of the sampling per se. In model calculations, we have been able to up-sample a minimal detector consisting of just 2×2 pixels by a factor of 32×32 , but this is computationally very expensive. This is akin to the quadrant detector method [23,24], although in the present case the probe can be large and does not define the resolution of the image.

We also note that when the properly sampled data is up-sampled, the reconstruction improves slightly [Fig. 3(d)], in this case reducing the halo effect around each particle. We suggest that the halos are due to partial coherence effects within the experiment and that as the pixel integration process is an incoherent sum of virtual subpixels, our method is allowing individual modes to be expressed on the subpixel level in the detector plane. This result suggests that the fidelity of all ptychographic images may benefit from a degree of diffraction plane up-sampling.

IV. CONCLUSIONS

We have shown here that the usual CDI sampling criterion does not apply to ptychography, even in the case where large detector pixels integrate significant regions of the diffraction pattern. We can obtain a good reconstruction when the fundamental ptychographic sampling is only just satisfied: in this case recovering a diffraction pattern which was undersampled according to the CDI criterion by a factor of 3×3 by using data with a ptychographical sampling factor of only 3.1×3.1 . The practical implication is that we can now engineer a probe function in any way we like without putting constraints upon the size of the detector, the number of pixels within it, or the specimen-detector distance. The results also have implications for the amount of data required for a ptychographical experiment: Any combination of probe step size and detector pixel size (in terms of its angle subtended at the specimen) that satisfies the fundamental ptychographic sampling can be employed, with pixel size being traded with probe step size in the object plane as desired. By allowing the detector to be positioned close to the sample, the possible resolution of the ptychograph obtainable for any given detector size, pixel size, or probe size can be greatly improved. In the example presented here, we have up-sampled by up to a factor of 12×12 , thus solving for 144 times as many detector pixels than originally measured. This scheme can be used to effectively increase the width of the modulation transfer function (MTF) of the detector indefinitely. Finally, we note that a reconstruction

from data that notionally fulfils the usual CDS condition can anyhow be improved upon by up-sampling, suggesting that this should be the normal practice when performingptychographic reconstructions.

ACKNOWLEDGMENTS

This work was funded by the EPSRC Doctoral Prize Fellowship and the EPSRC Basic Technology Grant No. EP/E034055.

-
- [1] M. Dierolf, A. Menzel, P. Thibault, P. Schneider, C. Kewish, R. Wepf, O. Bunk, and F. Pfeiffer, *Nature (London)* **467**, 436 (2010).
- [2] P. Trtik, A. Diaz, M. Guizar-Sicairos, A. Menzel, and O. Bunk, *Cement and Concrete Composites* **36**, 71 (2013).
- [3] B. Chen, M. Guizar-Sicairos, G. Xiong, L. Shemilt, A. Diaz, J. Nutterm, N. Burdet, S. Huo, J. Mancuso, M. Alexander, F. Vergeer, A. Burgess, and I. Robinson, *Sci. Rep.* **3**, 1177 (2013).
- [4] M. Beckers, T. Senkbeil, T. Gorniak, M. Reese, K. Giewekemeyer, S.-C. Gleber, T. Salditt, and A. Rosenhahn, *Phys. Rev. Lett.* **107**, 208101 (2011).
- [5] A. M. Maiden, G. R. Morrison, B. K. A. Gianoncelli, and J. M. Rodenburg, *Nat. Commun.* **4**, 1669 (2013).
- [6] M. Guizar-Sicairos and J. R. Fienup, *Opt. Express* **16**, 7264 (2008).
- [7] P. Thibault, M. Dierolf, O. Bunk, A. Menzel, and F. Pfeiffer, *Ultramicroscopy* **109**, 338 (2009).
- [8] A. M. Maiden and J. M. Rodenburg, *Ultramicroscopy* **109**, 1256 (2009).
- [9] J. Miao, P. Charalambous, J. Kirz, and D. Sayre, *Nature (London)* **400**, 342 (1999).
- [10] J. Miao, D. Sayre, and H. N. Chapman, *J. Opt. Soc. Am. A* **15**, 1662 (1998).
- [11] T. B. Edo, D. J. Batey, A. M. Maiden, C. Rau, U. Wagner, Z. D. Pesic, T. A. Waigh, and J. M. Rodenburg, *Phys. Rev. A* **87**, 053850 (2013).
- [12] Y. Chushkin and F. Zontone, *J. Appl. Crystallogr.* **46**, 319 (2013).
- [13] Y. Takahashi, A. Suzuki, S. Furutaku, K. Yamauchi, Y. Kohmura, and T. Ishikawa, *Appl. Phys. Lett.* **102**, 094102 (2013).
- [14] M. Guizar-Sicairos, M. Holler, A. Diaz, J. Vila-Comamala, O. Bunk, and A. Menzel, *Phys. Rev. B* **86**, 100103 (2012).
- [15] A. M. Maiden, M. J. Humphry, F. Zhang, and J. M. Rodenburg, *J. Opt. Soc. Am. A* **28**, 604 (2011).
- [16] A. M. Maiden, M. J. Humphry, and J. M. Rodenburg, *J. Opt. Soc. Am. A* **29**, 1606 (2012).
- [17] S. O. Hruszkewycz, M. V. Holt, C. E. Murray, J. Bruley, J. Holt, A. Tripathi, O. G. Shpyrko, I. McNulty, M. J. Highland, and P. H. Fuoss, *Nano Lett.* **12**, 5148 (2012).
- [18] C. Rau, U. Wagner, Z. Pei, and A. De Fanis, *Phys. Status Solidi A* **208**, 2522 (2011).
- [19] C. Ponchut, J. M. Rigal, J. Clment, E. Papillon, A. Homs, and S. Petitdemange, *J. Instrum.* **6**, C01069 (2011).
- [20] J. N. Clark and A. G. Peele, *Appl. Phys. Lett.* **99**, 154103 (2011).
- [21] P. Thibault and A. Menzel, *Nature (London)* **494**, 68 (2013).
- [22] S. Marchesini, A. Schirotzek, C. Yang, H. tieng Wu, and F. Maia, *Inverse Probl.* **29**, 115009 (2013).
- [23] M. N. Landauer, B. C. McCallum, and J. M. Rodenburg, *Optik* **100**, 37 (1995).
- [24] B. Hornberger, M. Feser, and C. Jacobsen, *Ultramicroscopy* **107**, 644 (2007).